ORIGINAL RESEARCH

Reoxygenation-Derived Toxic Reactive Oxygen/Nitrogen Species Modulate the Contribution of Bone Marrow Progenitor Cells to Remodeling After Myocardial Infarction

Nicanor I. Moldovan, PhD; Mirela Anghelina, MD; Saradhadevi Varadharaj, PhD; Omer I. Butt, PhD; Tiangshen Wang, PhD; Fuchun Yang, MD; Leni Moldovan, PhD; Jay L. Zweier, MD

***Background*—**The core region of a myocardial infarction is notoriously unsupportive of cardiomyocyte survival. However, there has been less investigation of the potentially beneficial spontaneous recruitment of endogenous bone marrow progenitor cells (BMPCs) within infarcted areas. In the current study we examined the role of tissue oxygenation and derived toxic species in the control of BMPC engraftment during postinfarction heart remodeling.

***Methods and Results*—**For assessment of cellular origin, local oxygenation, redox status, and fate of cells in the infarcted region, myocardial infarction in mice with or without $LacZ^+$ bone marrow transplantation was induced by coronary ligation. Sham-operated mice served as controls. After 1 week, $LacZ^+$ BMPC-derived cells were found inhomogeneously distributed into the infarct zone, with a lower density at its core. Electron paramagnetic resonance (EPR) oximetry showed that pO_2 in the infarct recovered starting on day 2 post–myocardial infarction, concomitant with wall thinning and erythrocytes percolating through muscle microruptures. Paralleling this reoxygenation, increased generation of reactive oxygen/nitrogen species was detected at the infarct core. This process delineated a zone of diminished BMPC engraftment, and at 1 week infiltrating cells displayed immunoreactive 3-nitrotyrosine and apoptosis. In vivo treatment with a superoxide dismutase mimetic significantly reduced reactive oxygen species formation and amplified BMPC accumulation. This treatment also salvaged wall thickness by 43% and left ventricular ejection fraction by 27%, with significantly increased animal survival.

***Conclusions*—**BMPC engraftment in the infarct inversely mirrored the distribution of reactive oxygen/nitrogen species. Antioxidant treatment resulted in increased numbers of engrafted BMPCs, provided functional protection to the heart, and decreased the incidence of myocardial rupture and death. **(*J Am Heart Assoc*. 2014;3:e000471 doi: 10.1161/JAHA.113.000471)**

Key Words: antioxidants • myocardial infarction • reactive oxygen/nitrogen species • stem/progenitor cells • ventricular rupture

In addition to resident stem/progenitor cells,[1,2] nonhematopoietic[3–5] and hematopoietic[6] bone marrow–derived cells also possess cardiogenic, vasculogenic, and fibrogenic capabilities. However, their potential could not be successfully applied to treat the sequelae of myocardial infarction (MI) because of our incomplete understanding of their in vivo behavior and also due to the poor receptivity of the deployment site.[7] Normally, the place of cell administration is the border zone of an infarct,[2] but the additional benefit of cell preconditioning triggered by hypoxia[8] or reactive oxygen species (ROS)[9] demonstrates that these factors also modulate the efficacy of cell therapy in infarcted hearts. However, the impact of the milieu at the core of the infarcts on survival and functions of either exogenous or endogenous cells with primitive characteristics and/or repairing capacity has not been fully investigated.

Stimulated recruitment of bone marrow–derived progenitor cells (BMPCs) is beneficial to postinfarction recovery.[3] In addition, the limitation of spontaneous BMPC engraftment in the hearts of c-Kit/CD117-knockout mice with permanent coronary ligation decreases postinfarction survival and contractile function, compared with wild-type controls.[10] These

From the Department of Internal Medicine/Division of Cardiovascular Medicine (N.I.M., J.L.Z.) and Davis Heart and Lung Research Institute (N.I.M., M.A., S.V., O.I.B., T.W., F.Y., L.M., J.L.Z.), The Ohio State University, Columbus, OH.

Correspondence to: Nicanor I. Moldovan, PhD, or Jay L. Zweier, MD, Davis Heart and Lung Research Institute, 460 W. 12th Ave, Columbus, OH 43210. E-mail: nicanor.moldovan@osumc.edu, jay.zweier@osumc.edu

Received August 16, 2013; accepted December 1, 2013.

effects could rely on direct differentiation and/or fusion with adult cardiomyocytes,[11] or paracrine mechanisms (including intercellular micro-RNA[12] or mitochondrial[13] transfer). The origin of cardiac myofibroblasts is also attributed to circulating precursors that originate in the bone marrow.[14,15] These myofibroblasts are no longer considered passive bystanders and/or generators of unwanted scarring, but contributors to an emergency repair process that mechanically stabilizes the ventricular cavity against rupture following infarction.[16] Clinically, immunosuppressive treatments lead to increased cardiac rupture.[17] Moreover, in a murine model of myocardial infarction (MI) macrophage depletion also impairs healing.[18] In this respect, we have shown that macrophages facilitate progenitor cell recruitment,[19] and others demonstrated that these cells affect differentiation-dependent functions of myofibroblasts via their secretion of metalloproteinases MMP-12[19] and MMP-28,[20] respectively. These data, along with others showing that BMPCs could adopt a cardiomyogenic fate in vivo,[21,22] argue for a supportive role of circulating BMPCs in maintaining the functioning and stimulating the repair and/or regeneration of the heart after infarction.

If left untreated larger heart infarcts often fail to heal, with common complications of left ventricular (LV) failure, rupture, and death. Unfortunately, the factors that limit the effects of BMPCs in post-MI recovery remain poorly understood. Severe myocardial hypo-oxygenation[23] and oxidative stress[24] are well known to occur during chronic ischemia, but the mechanisms have been studied so far mostly in the context of ischemia/reperfusion. Both these processes may limit the ability of BMPCs to successfully engraft, survive, and differentiate in a chronic infarct as well. Therefore, the goal of this study was to characterize how the alterations in myocardial oxygenation and oxidative stress modulate BMPC-mediated repair and how this repair process can be augmented through regulation of redox stress.

Methods

Bone Marrow Transplantation

All experiments were performed in accordance with the guidelines of the Office for Responsible Research and of the Institutional Animal Care and Use Committee (IACUC) of The Ohio State University. We used 12-week-old male mice expressing LacZ ("Rosa," 129-Gt[ROSA]26Sor; Jackson Laboratories, Bar Harbor, ME) as donors and age-matched wild-type controls as recipients. Bone marrow was harvested by flushing tibias and femurs of donor mice with RPMI 1640 medium (Life Technologies, Grand Island, NY) and filtered through a 40-μm nylon mesh (Miltenyi Biotec, Auburn, CA) to obtain a single cell suspension. Recipients were irradiated with 600 rads in 2 charges separated by 3 hours. Within 2 hours, the recipients were injected via tail vein with 5×10^6 bone marrow cells. For the next 4 days, these mice were injected intraperitoneally with 750 μL of PBS daily (to prevent dehydration) and allowed to reconstitute their hematopoietic system for 2 months. As a general rule, cells from 1 donor mouse were injected into 4 recipients.

Coronary Ligation

Mice with or without previous bone marrow transplantation were anesthetized with ketamine (55 mg/kg) and xylazine (15 mg/kg). Atropine (0.05 mg subcutaneously) was administered to reduce airway secretions. Animals were intubated and ventilated with room air (tidal volume, 250 μL; 120 breaths/min) with a mouse respirator (Model 845; Harvard Apparatus, Holliston, MA). A left intercostal thoracotomy was performed, and the left anterior descending coronary artery was ligated with a 7-0 silk suture. For each experiment, a similar number of sham-operated mice underwent the same surgery minus the coronary artery ligation. Rectal temperatures of the mice were maintained at 37°C by a Thermopad (Harvard Apparatus). Similar basal heart rates were observed in all animals, with values of 300 to 400 bpm, typical for anesthetized mice.

Antioxidant Treatment

For assessment of the effect of antioxidants on engraftment of BMPCs, we performed coronary ligation in 56 mice as described, of which 1 group of 14 mice had previously received bone marrow transplantation (BMT). After 24 hours, mice were randomly assigned to 2 equal-sized groups: 1 group was injected intraperitoneally with the superoxide dismutase/catalase mimetic (SODm) manganese (III) tetrakis (1-methyl-4-pyridyl) porphyrin (Alexis, San Diego, CA) at 25 mg/kg body weight in 0.5 mL of PBS, twice a day at 12 hour intervals, and the other group served as control (injected with PBS in the same conditions). The hearts of mice with BMT were collected and stained for β-galactosidase expression (vide infra), digital pictures were taken on a binocular microscope, and they were further used for various stainings, as described below. At the end of the experiment, the non-BMT surviving mice were euthanized, and their hearts were collected and fixed. One of the control mice died at surgery and was not used in this analysis.

Assessment of Myocardial Tissue Blood Flow

The fourth rib was removed after thoracotomy, and an optic suction probe (P10d; Moor Instruments, Wilmington, DE), connected to a laser Doppler perfusion monitor (Moor Instruments), was placed on the area at risk. Before and during coronary occlusion, regional myocardial blood flow was continuously monitored.

In Vivo EPR Oximetry

In one experiment, 10 μg of the oxygen-sensing spin probe lithium phthalocyanine (LiPc) microcrystals, synthesized electrochemically as described,[25] was loaded into a 26-gauge needle and implanted in the hearts of additional groups of sham-operated animals or in the midmyocardium of the core or within the border zone of the area at risk, after surgically exposing the hearts[26] (≥4 mice per condition). The O_2 response of LiPc showed good linearity from 0 to 114 mm Hg, with a sensitivity of 5.5 mGauss/mm Hg.[27] The electron paramagnetic resonance (EPR) spectra of LiPc crystals were obtained with the use of home-built or commercial (Magnettech, Berlin, Germany) L-band spectrometers with a frequency of 1.1 GHz, microwave power of 16 mW, modulation field of 0.045 G, and scan width of 3 G. After a 30-minute equilibration period, EPR oximetry was performed immediately before and after left anterior descending ligation, and on days 1, 3, 5, and 7, as previously described.[28]

LacZ Expression and Immunohistochemistry on Paraffin Sections

The presence of bone marrow–derived cells in the infarcted hearts was assessed after BMT and compared in 2 sets of mice: (1) mice with coronary ligation versus controls (sham-operated; n=7 per group); and (2) mice with coronary ligation with versus without antioxidant treatment (n=7 per group; see above). In all groups, 1 week after surgery mice were anesthetized and hearts collected and placed in Krebs buffer at 37°C. After 10 minutes the hearts were transferred into a fixative containing 2% formaldehyde and 2.5% glutaraldehyde in PBS for 24 hours at 4°C. For visualization of β-galactosidase expression, hearts were incubated overnight in basic X-gal solution (Amersham, Piscataway, NJ), pH 7.5,[29] then embedded in paraffin, and 4-μm sections were cut and used for hematoxylin and eosin staining, for immunohistochemistry, or for immunofluorescence. β-Galactosidase-stained sections (1 per heart per histochemical procedure) were further incubated with the antibodies anti-mouse F4/80 (AbD Serotec, Raleigh, NC), anti–troponin I, anti–smooth muscle actin, anti-ABCG2 (Abcam, Cambridge, MA), anti-Oct4 or anti–connexin 43 (Cell Signaling Technology, Danvers, MA) and processed with an ABC kit from Vector Laboratories (Burlingame, CA). Alternatively, when the LacZ staining was weak, heart sections were incubated with anti-lacZ antibody (Invitrogen Corp, Carlsbad, CA) followed by ABC. For collagen detection we performed Masson's Trichrome staining. Counterstaining for nuclear localization with maximum contrast was performed with hematoxylin or Fast Red as appropriate. For imaging we used a Nikon Eclipse E800 microscope (Nikon Corporation, Japan). Histological images were recorded on Kodak 35-mm positive slides that were then digitized with Nikon Supercoolscan 9000 (Nikon Corporation).

Engrafted BMPCs were also detected and probed using immunofluorescence with (1) fluorescein-labeled *Griffonia simplicifolia* lectin I–isolectin B4 (Vector Laboratories, Burlingame, CA), (2) anti-mouse NOS3, anti-mouse CD117/cKit or anti-NOS2 antibodies (Santa Cruz Biotechnology, Santa Cruz, CA), or (3) anti-nitrotyrosine antibody (Millipore, Billerica, MA), followed by secondary detection with Texas Red–conjugated antibodies (Santa Cruz). Nuclei counterstaining was done with 4′,6-diamidino-2-phenylindole (DAPI) (Invitrogen) and imaging was done with an Eclipse E800 microscope equipped with a CCD SenSys digital camera (Photometrics, Tucson, AZ) at 405-, 488,- and 595-nm excitation wavelengths.

Immunofluorescence on Frozen Sections

In a separate set of experiments, hearts from mice with MI and from sham-operated mice on days 1, 3, 5, and 7 after coronary ligation, as well as from mice with coronary ligation with or without manganese (III) tetrakis (1-methyl-4-pyridyl) porphyrin treatment in day 7 after surgery (n=3 per condition, per time) were embedded in optimum cutting temperature (OCT) and snap-frozen in liquid nitrogen. For immunocytochemistry, 5-μm frozen sections were treated as follows: (1) fixed at room temperature with 3.7% paraformaldehyde for 10 minutes, (2) permeabilized with 0.25% Triton X-100 in tris-buffered saline containing 0.01% Tween-20 (TBST) for 5 minutes, (3) blocked for 30 minutes with 1% BSA in TBST, (4) incubated with primary mouse anti-NOS2, rabbit anti-nitrotyrosine, or mouse anti-CD34-phycoerythrin in TBST+1% BSA for 1 hour at room temperature, and (5) incubated with the respective secondary goat anti-rabbit, Alexa Fluor 488–conjugated and goat anti-mouse, Alexa Fluor 586–conjugated antibodies (1:1000 dilutions) as necessary for 1 hour at room temperature. After thorough washing with TBST the sections were mounted in antifade mounting medium (Fluoromount-G, Birmingham, AL) and examined using an Olympus FV 1000 confocal microscope (Olympus America Inc, Melville, NY) with the ×10 or ×20 objective and with 405-, 488-, and 543-nm excitation for DAPI, green fluorescence, and red fluorescence, respectively.

For quantification of $NOS2^+$ and $CD34^+$ cells, 3 sections each from a different heart were analyzed, and 3 fields from the infarct area were acquired, with the same laser settings (using as controls unstained sections). Using Olympus FluoView Viewer v. 3.0 software, we measured the respective fluorescence intensity (arbitrary units) for each fluorophore, and the results were averaged for each condition.

ROS Detection

Whole mount staining of hearts

For assessing spatial distribution of ROS formation, we performed coronary ligation in 9 non–bone marrow trans-

planted C57/Bl6 mice as described. Then, at 1, 3, and 7 days the hearts from 3 mice per time point were collected from anesthetized animals injected with heparin, washed while beating in fresh Krebs buffer for 1 minute at 37°C, and then immersed in freshly made 2 mL of Krebs buffer containing 5 μmol/L 5-(and-6)-chloromethyl-2′,7′-dichlorodihydrofluorescein diacetate, acetyl ester (CM-DCF-DA) and 10 μmol/L dihydroethidine (DHE), which on reaction with superoxide converts to ethidium derivatives, fluorescent in red wavelengths[30] (both from Invitrogen Corp). Whole hearts were incubated at room temperature for 20 minutes and surface-imaged with ×1 or ×40 objectives in an Eclipse 800 microscope.

Measurement of ROS and redox buffering capacity in heart sections

ROS generation in OCT-embedded myocardial tissue from the same mice used for immunofluorescence (see above) was determined using DHE as described.[31] Briefly, one 5-μm-thick transverse section from each of 3 hearts per condition was covered with DHE (10 μmol/L in PBS) along with the nuclear stain Hoechst 33342—trihydrochloride, trihydrate (0.5 μmol/L). The slides were incubated in a light-protected chamber at 37°C for 30 minutes and mounted using Flouromount-G. Three to 5 images from each section were obtained using an Olympus FV 1000 confocal microscope with the ×10 or ×20 objectives at 405- and 543-nm excitation. Fluorescence intensity, which positively correlates with the amount of superoxide generation, was determined in the myocardial tissue from the infarcted areas, then quantified by automated image analysis using the Olympus software as described.

To identify the origin of superoxide, we incubated 3 additional sections from the same hearts, each with DHE as described but in the presence of either the SOD mimetic Mn (III)tetrakis(4-benzoic acid)porphyrin chloride (Alexis Biochemicals, San Diego, CA), the NADPH oxidase inhibitor VF244[32] (Molecules for Health, Richmond, VA), or the NOS2 inhibitor L-NIL (Caymen, Ann Arbor, MI) at 100 and 50 μmol/L. Fluorescence intensity was measured as described and averaged for 3 to 5 images per section; 3 hearts per condition were analyzed. The remaining signal in the presence of Mn(III) tetrakis(4-benzoic acid)porphyrin chloride was considered nonspecific (background signal), and therefore was subtracted from all other mean intensities in control, VF244 treated, and L-NIL treated sections.

Whole-Organ Image Analysis

Whole hearts from 4 mice with coronary ligation and manganese (III) tetrakis (1-methyl-4-pyridyl) porphyrin treatment and 3 mice with coronary ligation and PBS treatment after bone marrow transplantation, as described, were stained for LacZ expression as described, and they were photographed with a Nikon stereomicroscope. MetaMorph was used to find the differences in the intensity of blue staining by (1) color separation and (2) analysis of inverted blue channel. Infarct region was then contoured on this image, integrated pixel intensity was divided by the region area, and average pixel intensities thus calculated were used for various comparisons.

Determination of Heart Function by Magnetic Resonance Imaging

Mice were imaged on an 11.7-T (500 MHz) magnetic resonance microimaging system with Bruker Advance console, using an radiofrequency probe with an inner diameter of 2.8 cm and shielded micrograd ients capable of 100 G/cm and 110-μs rise time (Bruker Biospin, Ettlingen, Germany). Tuning and matching the probe, slice-selective shimming and flip-angle calibration were performed manually before each experiment. Scout imaging for long- and short-axis orientation of the heart, using a k-space segmented cardiac-triggered and ECG-gated gradient-recalled echo fast low-angle shot sequence, was performed. Six to 7 contingent slices (slice thickness, 1 mm) were then acquired in short-axis orientation covering the entire heart. Images were acquired with the following parameters: field of view (FOV), 25 mm; slice select thickness, 1 mm; matrix size, 256×256; TE/TR, 1.6/5.0 ms; and radiofrequency Gaussian excitation pulse, 30°. Standard Bruker scouting images were used to locate the heart. Acquisition of multiple axial short-axis slices covering base to apex was done in <30 minutes. An inhouse image analysis algorithm as reported previously[33] allowed quantification of both heart morphometry and wall motion following experimental infarction, from which cardiac output was determined. Six mice per treatment condition (SODm or vehicle control) were anesthetized with 1% isoflurane in room air at a 2.0 L/minute flow rate, positioned within a cradle containing a built-in nose cone for isoflurane delivery and placed in the RF coil tuned to 500 MHz. The ECG signals obtained from the subcutaneous leads were used to provide external triggering of fast gradient echo cine imaging sequences. Body temperature was maintained at 37°C through a rectal thermoprobe controlling an external heating unit. A respiration pad placed between the cradle and the thoracic cage was used to monitor breathing rate.

Data Analysis

The statistical significance of differences for various comparisons was determined with the 1-tailed Student *t* test using built-in routines in Excel 2010 and Minitab Statistical Software (Minitab, Inc 2009, State College, PA). $P<0.05$ was considered statistically significant. Because the sample size

was small in some experiments (3 to 6 animals), we also performed the nonparametric Mann–Whitney test (Wilcoxon rank sum test). In all instances, the *P* values confirmed the level of significance obtained with the *t* test. Kaplan–Meier survival analysis was done with IBM SPSS Statistics v. 19 (IBM Corporation, Armonk, NY). Data are expressed as mean±SD, as indicated in figure legends.

Results

Pattern of BMPC Recruitment and Differentiation in the Infarcted Heart

In mice transplanted with LacZ-expressing bone marrow, whole-heart ß-galactosidase staining 7 days after coronary ligation allowed direct assessment of the distribution of BMPCs recruited into the ischemic at-risk zone (Figure 1). Given the very thin and transparent mouse epicardium, this staining (which appears blue) is representative of muscle colonization with BMPCs, as confirmed by cross-sectional histology (Figure 2) and also shown by others.[34] As expected, in control hearts (without coronary ligation), the staining for LacZ was absent (Figure 1A), whereas in the infarcted myocardium $LacZ^+$-positive BMPCs were abundant yet variably distributed in a band starting from the border zone and expanding to the ischemic core. This produced a rim of dense β-galactosidase expression, but the infarct core was variably stained (Figure 1B and 1C). As shown below, this staining variability persists over time and arises because of active detrimental processes limiting BMPC survival. Overall, $LacZ^+$ cell accumulation had an inverse relationship with the extent of LV remodeling (compare Figure 1B and 1C), in accordance with previous findings.[35]

Distribution of $LacZ^+$ cells in heart sections followed the pattern seen on the surface, with a preferential localization starting at the interface between the healthy and ischemic tissue. In sections of nonischemic myocardium of infarcted hearts, cardiomyocytes were uniformly labeled by the anti–troponin I antibody in a banded pattern (Figure 2A). Troponin I immunoreactivity was fainter and uneven in cardiomyocytes of the border zone (Figure 2B). In line with previous data suggesting the cardiomyogenic potential of BMPCs,[21,22] clusters of $LacZ^+$ cells were occasionally found in a perivascular location (Figure 2B). These cells with relatively little cytoplasm and larger nuclei than nearby vascular and inflammatory cells were integrated with mature cardiomyocytes that demonstrated weak troponin I staining. In the border zone we also observed compact patches of $LacZ^+$ cells (blue) intermixed with small troponin I–positive (brown) and –negative cells (Figure 2C). Of note, the size of cardiac precursor cells, in addition to their molecular composition, remains a valuable criterion for differentiation status on cardiomyocyte lineage.[36]

One week after infarction, polymorphonuclear leukocytes were largely absent. However, we could identify in the infarct zone monocytes/macrophages double-positive for LacZ and F4/80, a mouse macrophage marker (Figure 2D), and LacZ/smooth muscle actin double-positive cells with a morphology of myofibroblasts (Figure 2E). Signs of fibrosis were minimal at this time, the deposits of organized collagen fibrils being mostly limited to the surface (Figure 2F).

We also found occasional immunoreactivity for connexin 43, mostly in areas in contact with adult cardiomyocytes (Figure 2G). Immunostaining also revealed abundant stem/progenitor cell markers in the infiltrating cell population, illustrated by the expression of ABCG2/CD338 (Figure 2H)

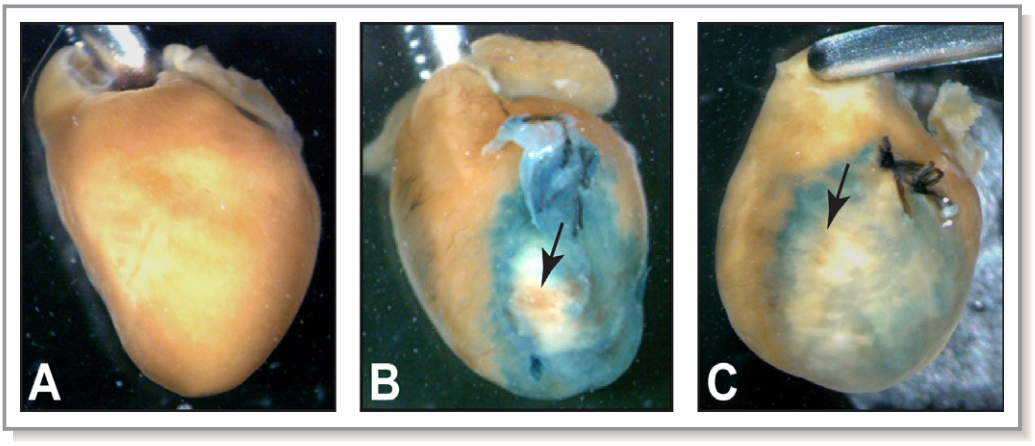

Figure 1. Pattern of engraftment and repair activity of bone marrow progenitor cells (BMPCs) in experimental infarction after bone marrow transplantation. A, Staining of a heart without coronary ligation. B and C, Hearts with coronary ligation for 1 week (replicates). Note the band-like accumulation of bone marrow–derived cells at the interface of the normal and ischemic zones and the inverse relationship between the quantity of bone marrow cells and the amplitude of cardiac remodeling; arrows indicate superficial hemorrhages in the BMPC exclusion zone. All hearts (n=7 per group) were simultaneously incubated in the β-galactosidase substrate (blue color).

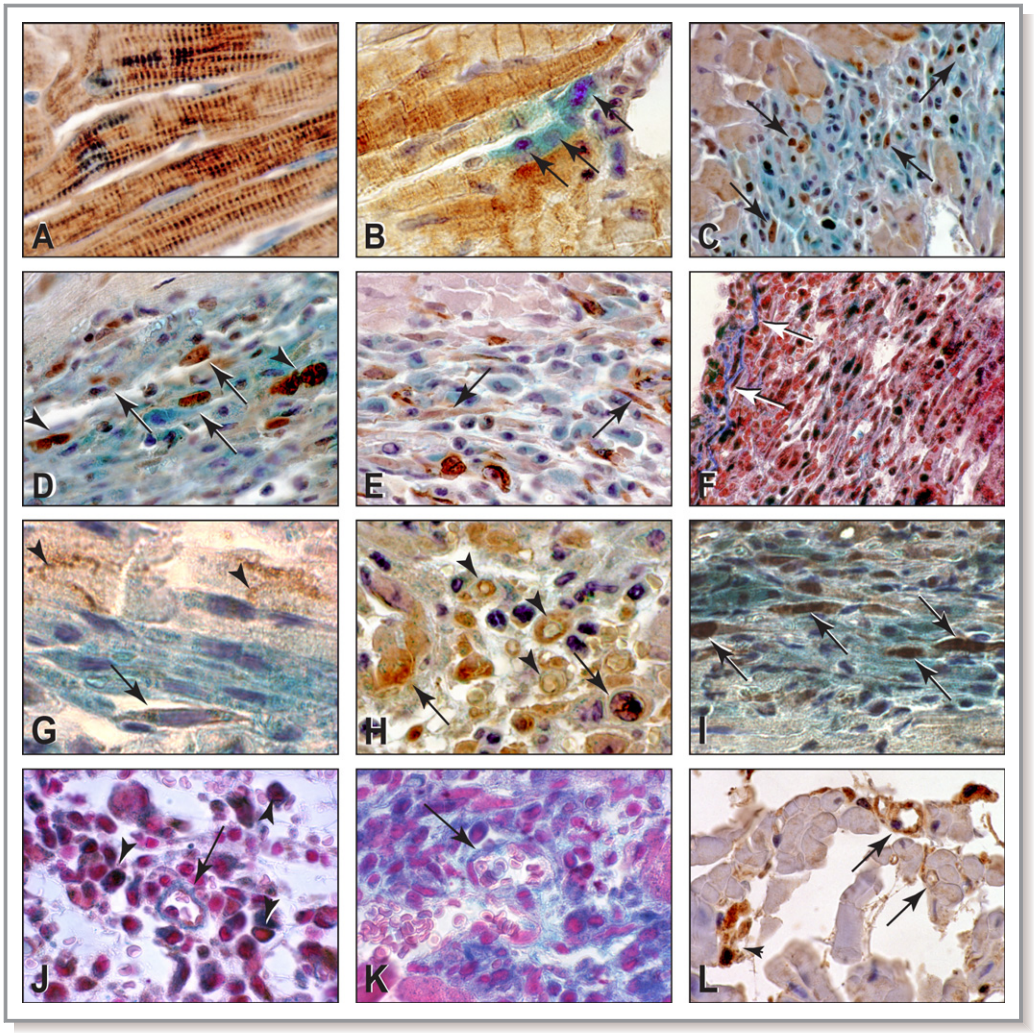

Figure 2. Cellular composition of the myocardium 1 week post-MI. A through C, Anti–troponin I immunostaining. A, Noninvolved myocardium in an infarcted heart, with intense, striated labeling of cardiomyocytes (pale blue color represents nuclei stained with hematoxylin). B, Cluster of $LacZ^+$ bone marrow–derived cells (bright blue/cyan in the cytoplasm, arrows) adjacent to a blood vessel, apparently in the process of integration with preexistent cardiac myofibers in the infarct border zone. Troponin I expression is weaker and nonuniform in this region, indicative of the ischemic state of the myocardium (same heart as in A). C, Mosaic distribution of $LacZ^+$ cardiomyocytes (troponin I^+), arrows, in a cluster of BMPCs in the border zone. D, Cells expressing the mouse macrophage marker F4/80 (arrows), with some grouped in pairs (arrowheads), interspersed with other $LacZ^+$ bone marrow–derived cells. E, Cells with a myofibroblast morphology (arrows) displaying a yellowish color as a result of the overlay of LacZ staining (pale blue) and anti–smooth muscle actin (brown). F, Collagen deposition visualized by Trichrome staining. In the infarct core at 7 days, only a few mature collagen fibers (blue staining) are present, mostly in the epicardial layer (arrows). G, Expression of connexin 43 in an infarct-recruited $LacZ^+$ cell (arrow, brown staining). The banded staining for connexin 43 is also detectable at the interfaces between adult cardiomyocytes (seen in oblique section, arrowheads). H, Expression of primitive marker ABC-G2 detected by immunostaining (brown) in isolated mononuclear cells (arrows) and in double-positive LacZ/ABC-G2 microvessels containing erythrocytes (arrowheads). I, Imunonodetection of the primitive cell marker Oct4 in infiltrating mononuclear cells (brown, arrows). J, LacZ-positive blood vessel (arrow) in a field containing many c-kit/CD117 (brown)/$LacZ^+$ (blue) bone marrow–derived double-positive cells (arrowheads). K, Negative control for J, with Fast Red as nuclear counterstain (J). The arrow points to $LacZ^+$ cells in a microvessel (identified by the presence of erythrocytes). L, Immunostaining for β-galactosidase expression in microvessels (brown, arrows). The antibody also detected clusters of mononuclear cells (arrowhead). The hearts (n=5 for coronary ligation; n=4 for sham-operated mice) were the same as those used in Figure 1. A through I and L, counterstaining with hematoxylin. Original magnifications: A through E and G through K, ×200; F and L, ×120. BMPC indicates bone marrow progenitor cell; MI, myocardial infarction.

and Oct4 (Figure 2I), which are "side population" and embryonic markers, respectively, as well as c-Kit/CD117 (Figure 2J, arrowheads). In addition, in the border zone many cells in small- and medium-sized microvessels expressed LacZ, indicative of ongoing neovascularization with contribution of bone marrow cells (Figure 2J and 2K, arrows). This process was confirmed by the presence of β-galactosidase by direct immunodetection in microvessels and in clusters of infiltrating cells (Figure 2L), as expected from the direct LacZ staining.

Structural Correlates of BMPC Distribution

We questioned why the pattern of BMPC engraftment is limited to a band covering the transition from classical "border zone" to within the "at risk" region, with a reduction at the central core. We observed that LacZ$^+$ cells were largely absent from regions that contained intramural hemorrhages, seen on the surfaces of most hearts (Figures 1B, 1C, and 3A). This segregation of areas containing BMPCs from those containing mostly mural erythrocyte pools, both of blood origin, suggested that the mechanism of these cellular recruitment events must be different. Indeed, locations of blood pools were more central to the infarcted areas or at the interface of bone marrow cell–devoid areas with LacZ-expressing zones (Figure 3A). Occasionally, hemorrhages were accompanied by ventricular aneurysms (Figure 3B), suggesting the mechanical failure of the tissue. Microscopically, in the LacZ-positive zones erythrocytes were often contained within thin β-galactosidase-expressing neovascular profiles (Figure 2J and 2K). However, an abundance of free erythrocytes was also found deeper in the infarct area, with an unexpected increase in frequency toward the LacZ-negative core (Figure 3A). Microscopically, the erythrocytes were often found in extravascular pools, associated with sites of muscle ruptures (Figure 3B and 3C). Their morphology was intact, with uniform density of hemoglobin. Combined with the absence of hemosiderin deposits in macrophages, these observations suggested that the origin of the fresh blood "lakes" was directly from the LV cavity, as confirmed by histology (Figure 3D). Collectively, these observations showed that the fresh blood pools corresponded to the hemorrhages observed on the surface of hearts and represented percolation of erythrocytes derived from microvascular and/or muscle ruptures. Indeed, in the current study ≈60% of untreated mice died post-MI, mostly from ventricular rupture documented at autopsy, in line with previous results.[37] Another key observation was that in the thinned regions of the ischemic myocardium the majority of cells remaining to protect the muscle from disintegration (Figure 3D) were noncardiomyocytes, many staining for smooth muscle-type alpha actin (Figure 2E) and/or primitive markers (Figure 2G through 2J). These findings suggest that BMPCs, as originators of the myofibroblast pool,[14,15] may have a role in biomechanical stabilization of necrotic myocardium, possibly even before collagen deposition in the postinfarction scar (Figure 2F).

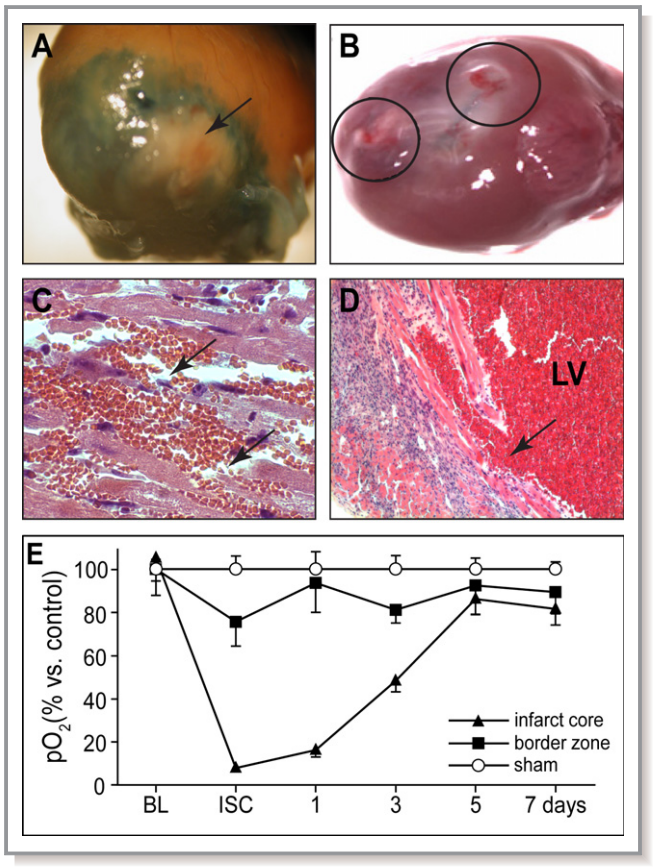

Figure 3. Ventricular microruptures and microhemorrhages as originators of passive reoxygenation in infarcted hearts. A, Hemorrhages seen from the ventricular surface in the BMPC-devoid core of the infarct (arrows). B, Hemorrhages were often associated with ventricular aneurysms in the infarct area (encircled). C, Extensive mural hemorrhage (arrows) and ventricular ruptures in an infarct area. D, Apparent origin of percolating erythrocytes from the left ventricular (LV) cavity (arrow). Note the reliance of cardiac wall integrity in this area mostly on the bone marrow–derived infiltrating cells (blue). Original magnifications: C, ×120; D, ×40. E, Postinfarction myocardial oxygenation assessed by in vivo EPR oximetry. Mice (n≥4 per group) were implanted with an LiPc oximetry probe either in the border zone (squares) or at the core of the infarct (triangles). Sham-operated mice (n=5) served as controls (open circles). For direct comparison, data are expressed as percentage of the pO_2 values detected in sham-operated mice, on the corresponding day postimplantation. The actual values of myocardial pO_2 during sham surgery or before coronary artery occlusion were 19±1 and 20±2 mm Hg, respectively. BL indicates before ligation; BMPC, bone marrow progenitor cell; ISC, ischemia, immediately after ligation; further on the abscissa, days after coronary ligation; LiPc, lithium phthalocyanine. Data are presented as mean±SD. EPR denotes electron paramagnetic resonance.

Passive Reoxygenation of Infarcted Regions After Coronary Ligation

The observation that erythrocytes were present in the infarcted myocardium but were inversely correlated with the distribution of BMPCs prompted us to measure oxygenation in the ischemic hearts. To this end, we used EPR oximetry to measure pO_2, with implantation of oximetry probe LiPc[25] microcrystals at the time of coronary ligation into the area at risk and into the border zone. We found that immediately after coronary ligation oxygen levels decreased from ≈20 to

<2 mm Hg in the central zone. However, the low pO_2 in this location began to reverse after 24 hours, with about half recovery to baseline levels after 3 days and almost full recovery by day 5 postinfarction (Figure 3E). pO_2 detected in the border zone remained only marginally lower than that in control animals.

Origin and Consequences of ROS and RNS Generated in Infarcted Myocardium

Next, we hypothesized that the spontaneous reoxygenation of the ischemic tissue at the infarct core could trigger increased free-radical generation in a manner similar to classical ischemia-reperfusion,[38] and this might limit BMPC accumulation in central areas of the infarct. To test this possibility, we first detected ROS formation and distribution using whole-heart incubation with ROS-sensitive fluorescent probes DHE (sensitive to superoxide[39]) and CM-DCF-DA (sensitive to H_2O_2 and other ROS[40]), and we compared their pattern with that of LacZ staining. We found that at the core of infarcts there was substantial DHE-detectable superoxide formation, accompanied by a time-dependent increase of CM-DCF-DA staining (Figure 4A through 4I) in a pattern visible from the surface and inversely mirroring the distribution of $LacZ^+$ bone marrow–derived cells (Figures 1B and 3B).

To assess the origin of ROS in the infarcted hearts, we preincubated the heart sections in the presence or absence of inhibitors of ROS-generating enzymes and then performed ROS measurements with the addition of DHE (Figure 5A). In nontreated sections, we found that average DHE fluorescence intensity increased over the 7 days post-MI (Figure 5A, column labeled "DHE"). This signal was largely abolished by SODm, confirming that it was secondary to superoxide (Figure 5A, column "Background"). Slides pre-incubated with

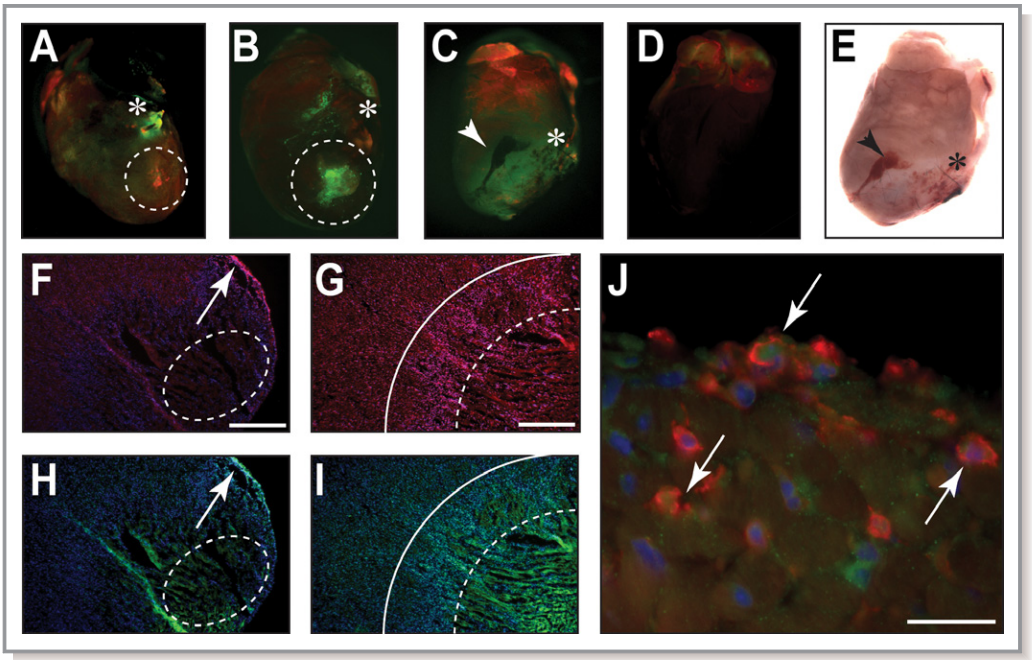

Figure 4. Imaging ROS formation in infarcted hearts. A through D, Whole-mount fluorescence imaging of ROS formation with CM-DCF-DA (green) and DHE (red) in hearts after infarction (location of coronary ligation identified by the star). A, Heart at 1 day: a small surface spot is positive for the 2 probes (dashed white circle). B, Heart 3 days after coronary ligation; note the increased size and intensity of the CM-DCF-DA-positive spot (dashed circle). C, Infarcted heart at 7 days, showing further expansion of green fluorescence area. D, Opposite side of the same heart as in (C), where no green fluorescence in the ventricular region is seen (control for staining in A through D; the atria also show residual fluorescence, either as effect of surgical manipulation at coronary ligation and/or as autofluorescence). E, Optical imaging of the same heart as in (C); ligation point shown by star, identifies mural hemorrhages corresponding to the absence of staining in (C) consistent with the H_2O_2- and RNS-scavenging activity of hemoglobin[41] (arrowheads in C and E). F, Cryosection from a heart 3 days after coronary ligation stained with DHE and counterstained with DAPI. Note the bright staining on the heart surface (arrow, compare with H), corresponding to exposure of a band of higher intensity (limited by the highlighting lines in G). G, DHE staining seen in the midmyocardial border zone. In these sections, the core of the infarct (right from dashed lines) has a paucity of staining because of the low density of the nuclei. The solid and dashed lines approximate the border zone. H and I, Corresponding CM-DCF-DA staining of the sections in F and G. J, Cells double-positive for *Griffonia simplicifolia*-FITC lectin (green) and eNOS (red, arrows), present in the infarct border zone 7 days after coronary ligation. From each of the 3 hearts per condition 3×5-μm-thick transverse sections were analyzed. Original magnifications: F through I, ×20; J, ×40. Bars: 50 μm. CM-DCF-DA indicates 5-(and-6)-chloromethyl-2′,7′-dichlorodihydrofluorescein diacetate; DAPI, 4′,6-diamidino-2-phenylindole; DHE, dihydroethidine; eNOS, NOS3 (nitric oxide synthase, endothelial); FITC, fluorescein isothiocyanate; RNS, reactive nitrogen species; ROS, reactive oxygen species.

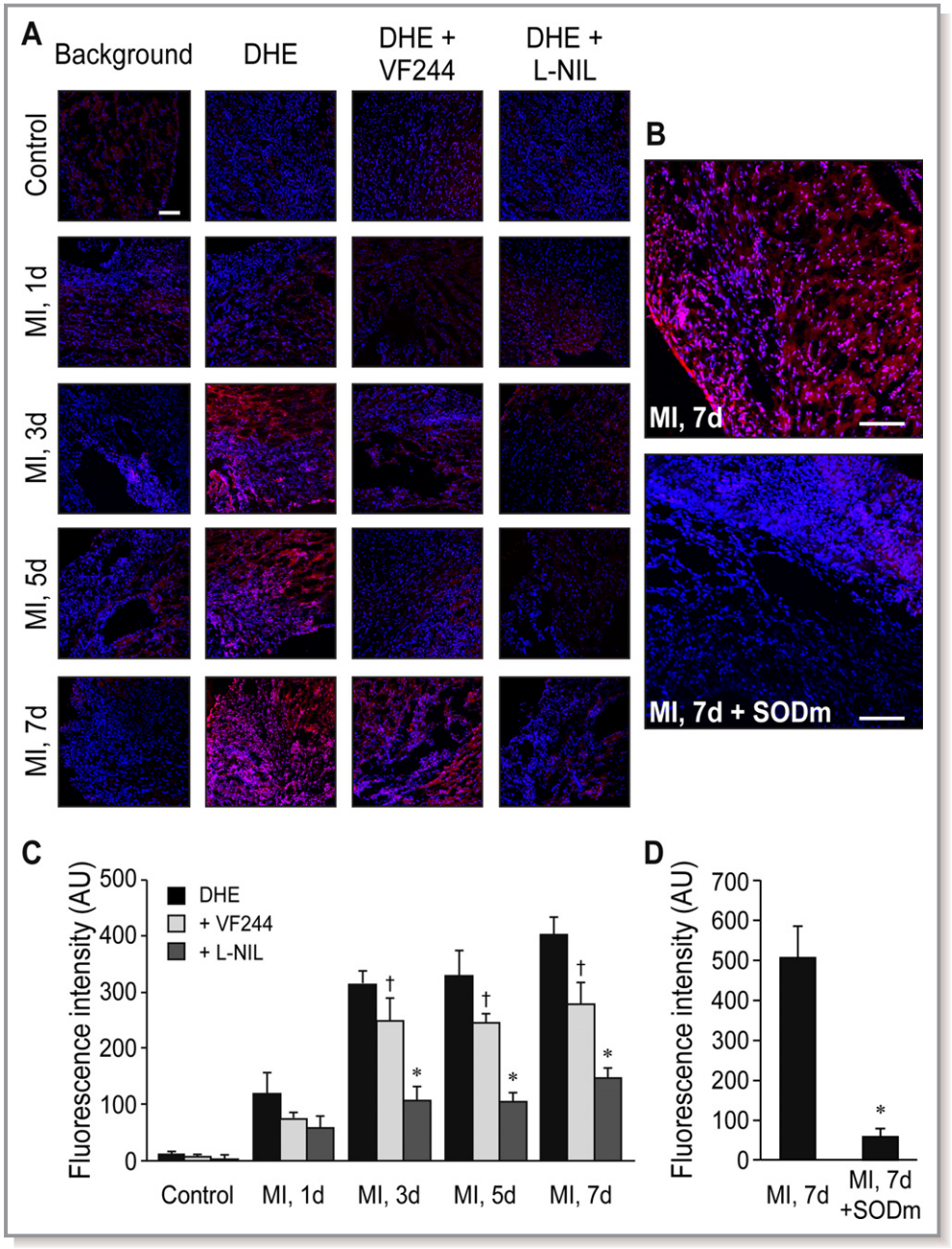

Figure 5. Time course and source of superoxide generation in heart tissue during chronic ischemia. A, Representative fluorescence photomicrographs of confocal optical sections of left ventricle myocardium labeled with DHE and counterstained with DAPI for nuclei. Each panel shows infarcted regions with infiltrated cells and adjacent myocardium. Original magnification: ×20; bar, 100 μm for all images. B, Effect of in vivo treatment of mice with the SOD mimetic MnTMPyP (SODm). Representative images of frozen sections of LV myocardium from SODm-treated and untreated mice after 7 days of coronary ligation, labeled with DHE. Each panel shows infarcted regions with infiltrated cells and adjacent myocardium. Bars, 100 μm. C, Intensity of DHE fluorescence measured from the corresponding left ventricle sections of controls and MI at 1, 3, 5, and 7 days, (DHE) and after pretreatment of sections with the NADPH oxidase inhibitor VF244 (+VF244) or the NOS2 inhibitor L-NIL (+L-NIL). Displayed results are based on subtraction from all values of the residual background fluorescence after treatment of the sections with the SODm MnTBAP (background column in A). Values are means±SD per each condition (arbitrary fluorescence units), n=3 to 5 images per section from 3 sections, each from a different heart. †P<0.05 VF244 vs untreated (DHE) MI groups; *P<0.01, L-NIL vs untreated (DHE) MI groups. D, Total intensity of DHE fluorescence measured from the corresponding left ventricle sections of MI at 7 days from controls (PBS treated) and SODm-treated mice. Values are means±SDs (in arbitrary fluorescence units per microscopic field, n=3 to 5 images per section, from 3 sections, each from a different heart); *P<0.001. DHE indicates dihydroethidine; L-NIL, N6-(1-iminoethyl)-L-lysine, dihydrochloride; LV, left ventricular; MI, myocardial infarction; MnTBAP, Mn(III)tetrakis(4-benzoic acid)porphyrin chloride; MnTMPyP, manganese (III) tetrakis (1-methyl-4-pyridyl) porphyrin NADPH, nicotine adenine dinucleotide phosphate, reduced; NOS2, nitric oxide synthase, inducible; PBS, phosphate buffered saline; SOD, superoxide dismutase.

saturating concentrations of the NADPH oxidase inhibitor VF-244[32] also showed reduced fluorescence (Figure 5A, column "+VF244"). Furthermore, the fluorescence could be almost completely blocked by L-NIL, a selective NOS2 inhibitor[41] (Figure 5A, column "+L-NIL"). These observations suggest that NOS2 is another major source of superoxide in this tissue, most likely via "uncoupling." Recently we[42] and others[43] have demonstrated that NOS uncoupling with a switch from NO generation to superoxide production occurs in ischemic myocardium. Because the DHE signal in 1-day ischemic hearts did not respond to the above inhibitors (Figure 5C), one may assume a different origin of early ROS formation. As previously reported, the mitochondrial electron transport chain, xanthine oxidase, and uncoupled endothelial form of NOS (NOS3) all can give rise to superoxide formation during the process of ischemic or postischemic injury.[44] In this regard, we also found numerous isolated, lumen-less infiltrating cells positive for NOS3 in the infarcted region, concurrent with positivity for *G. simplicifolia* isolectin B4[45] (Figure 4J).

We also tested if in vivo inhibition of ROS formation can protect BMPC engraftment by treating the mice with SODm. This was injected intraperitoneally starting 24 hours after coronary occlusion to prevent interference of the treatment with the early inflammatory response, which is also ROS dependent.[46] In sections obtained from the hearts of these SODm-treated mice DHE fluorescence was very low (Figure 5B and 5D, "MI, 7 days+SODm"), as opposed to hearts from untreated control mice (Figure 5B and 5D, "MI, 7 days"; semiquantitative data graphed in Figure 5D). This supports the notion that ROS are the source of the fluorescence signal seen and confirms that pharmacologic manipulation of ROS within the infarcted hearts by in vivo administration of an antioxidant is possible.

The presence of NOS2 in the infarcted hearts was directly assessed by immunochemistry. In the current study, normal hearts showed only trace immunostaining for NOS2 (Figure 6A), whereas after coronary ligation anti-NOS2 immunostaining in the infarct significantly increased by day 3 and then continued to rise to day 7 (Figure 6B through 6E). Reaction of superoxide and NO is known to produce the highly reactive oxidant peroxynitrite, which combines with tyrosyl residues in proteins and produces the adduct 3-nitrotyrosine (NT), which is toxic for infarct-accumulating circulating cells,[47] including those with progenitor character.[48] Indeed, the frequency of small (noncardiomyocytes) NT-positive cells increased in a time-dependent fashion in infiltrated areas (Figure 6B through 6E). As expected, the number and tissue density of these NT-positive cells was much lower in sections from mice 7 days post-MI that were treated with SODm (Figure 6F and 6G). To verify whether reactive oxygen/nitrogen species (ROS/RNS) formation affects the survival of progenitor cells and the relationship of this to NT formation, slides stained with an anti-NT antibody and counterstained with DAPI were further analyzed for nuclear morphology. In the same areas displaying NOS2 immunoreactivity, we also found small (ie, circulation-derived) cells positive for the NT adduct, displaying condensed (picnotic) or fragmented nuclei, both features of apoptosis (Figure 6H), consistent with a prior study focused on this topic.[47]

Next, to assess the impact of ROS-derived toxicity on the cellular dynamics in the infarcted hearts, we studied the kinetics of $CD34^+$ cell recruitment (Figure 7A through 7F), a cell class that represents bone marrow–derived progenitors for both endothelial cells[49] and myofibroblasts.[14] These cells substantially accumulated over the first 3 days postinfarction, but plateaued on day 5, and at 1 week their numbers declined back to levels of day 1 postinfarction (Figure 7G). Consistent with ROS-induced limitation of cell survival, in vivo treatment of mice with SODm almost doubled the density of these $CD34^+$ cells in the infarcted hearts compared with nontreated controls (Figure 7G).

Functional Benefits of Pharmacological Inhibition of ROS/RNS Formation in Infarcted Hearts

The animals treated with SODm after infarction showed remarkable improvement in survival (Figure 8A). In addition, SODm treatment also increased the coverage of the ventricular wall with BMPCs as seen from the surface (Figure 8B versus 8C) and detected by the surface density of LacZ staining in hearts from mice subjected to bone marrow transplantation (Figure 8D). Coincident with the increased number of recruited progenitor cells, SODm treatment also had beneficial structural and functional consequences as measured by cardiac magnetic resonance imaging. Decreased LV wall thinning at the infarct was seen with ≈43% greater minimum LV wall thickness with SODm treatment (Figure 8E) and cardiac output was ≈27% higher (Figure 8F). Postmortem anatomical evaluation indicated that the improved survival derived primarily from the increased minimum wall thickness with resistance to cardiac rupture.

Discussion

Intervention-based revascularization in some coronary artery disease patients is not always possible; therefore, the native capacity of the heart to sustain chronic ischemia and to undergo even a limited recovery is of great importance.[50] Clinical practice shows that the hearts of certain MI patients could spontaneously recover not only functionally but structurally as well.[51] Therefore, the intrinsic regenerative potential of the heart could be further amplified by cellular or

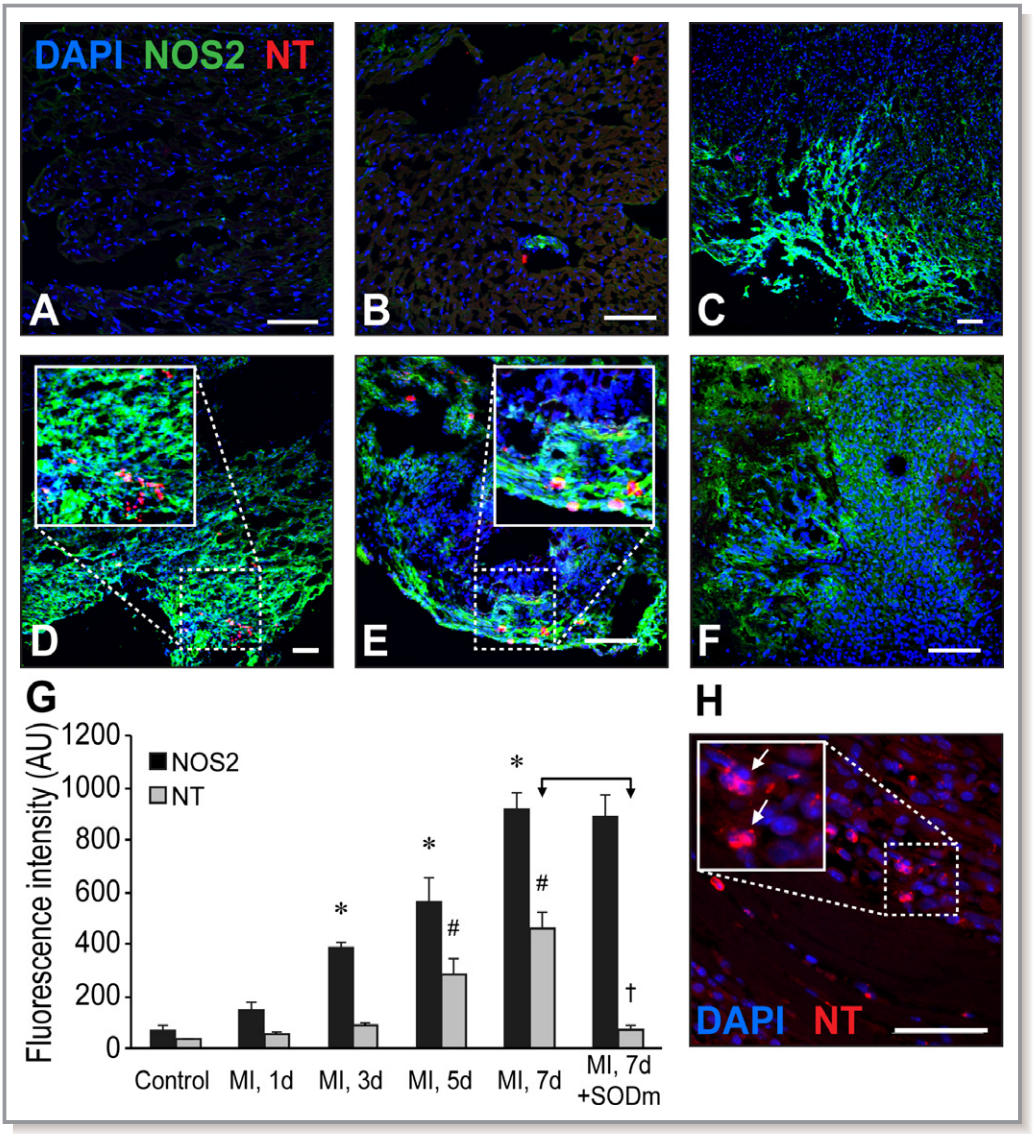

Figure 6. Distribution of NOS2 and 3-nitrotyrosine (NT)–producing cells in myocardia of mice subjected to coronary ligation. Representative sections of the hearts probed for NOS2 (green fluorescence) and NT (red fluorescence) in controls (A), after 1 day (B), after 3 days (C), after 5 days (D), and after 7 days (E), and at 7 days in the hearts of animals treated with SODm (F). Insets show higher magnifications of the cells within dashed squares. Bars: 100 μm. G, Semiquantitative assessment of the corresponding NOS2 antigen by immunofluorescence. Values are mean±SEM (n=3 to 8 sections from 3 different hearts); *P<0.05, NOS2 vs control; #P<0.05, NT vs control; and †P<0.01, myocardial infarction (MI), 7 days+SODm vs MI, 7 days. H, Strong NT immunostaining (red) in cell fragments and in the cytoplasm of mononuclear cells recruited into the infarct area. Inset: Concurrent apoptosis, revealed by nuclear fragmentation and shrinkage (picnosis; blue) taking place in NT-positive cells (arrows).

pharmacological interventions,[52] although numerous uncertainties persist regarding the actual processes involved.[53] In circulation there are cells known to be largely derived from bone marrow, with release stimulated by acute injury, such as in MI.[54] Therefore, the factors that modulate circulating stem/progenitor cell engraftment need to be better understood. The effects of tissue oxygenation, the redox state, and oxidative stress on this process of myocardial regeneration and healing are not known in sufficient detail. To address these critical questions, we studied the process of spontaneous BMPC recruitment in a mouse model of coronary occlusion in relationship to myocardial oxygenation and ROS/RNS formation.

This study demonstrates the following important findings: (1) recruitment of large numbers of BMPCs occurs in compact areas mediating myocardial and vascular repair post-MI, along with stabilization of the thinned necrotic myocardium against mechanical disintegration; (2) this process is limited to a banded region partially overlapping but larger than the infarct's classical "border zone"; (3) delayed myocardial

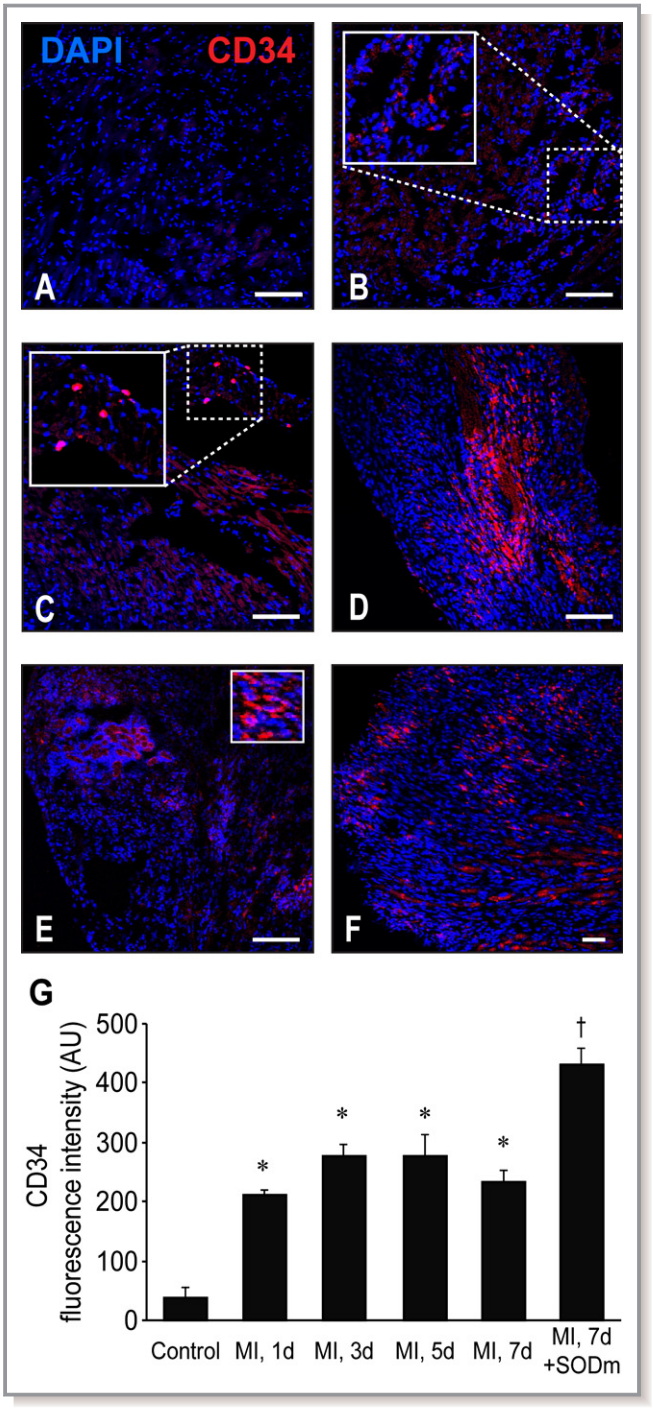

Figure 7. Dynamics of CD34$^+$ progenitor cell recruitment in post-myocardial infarction (MI) mouse hearts. The hearts were subjected to LCA ligation for 1 day (B), 3 days (C), 5 days (D), and 7 days (E). A, Control. F, MI at 7 days in animals treated with SODm. Representative sections of the hearts probed by immunofluorescence for CD34 (red); nuclei (blue). Insets show higher magnifications of the cells within dashed squares. Bars: 100 μm. At 7 days, circular profiles (E, inset) suggest endothelial differentiation (compare with Figure 1H). G, Quantification of total CD34 fluorescence intensity. Values are mean±SD (n=3 sections, each from a different heart); *P<0.01 vs control; †P<0.001 MI, 7 days+SODm vs MI, 7 days. LCA indicates left coronary artery.

reoxygenation occurs in the infarct core, triggering enhanced ROS/RNS formation; (4) ROS/RNS-induced cytotoxicity controls the distribution and thus the limited engraftment of BMPCs; (5) ROS/RNS formation can be countered by administration of an antioxidant SOD mimetic, resulting in enhanced BMPC accumulation coincident with improved cardiac function and increased postinfarction survival with decreased incidence of ventricular rupture, a main mechanism of death after coronary ligation in mice.[55]

Pattern of BMPC Infiltration

At 1 week postinfarction, which corresponds to the peak of BMPC recruitment,[56] the signs of fibrosis were still minimal, but we found many LacZ$^+$ cells (ie, of bone marrow origin), with cardiomyogenic, neovascular, and fibrogenic commitment, similar to studies using eGFP-labeled bone marrow cells.[57,58] The localization of these BMPCs within the risk region was preferentially in a large but variable band at the interface of normal with damaged tissue, where these cells appeared more differentiated (as microvessels, macrophages, and patches of LacZ$^+$–troponin I$^+$ cells). Toward the infarct core, these BMPCs were detectable mostly as myofibroblasts (LacZ$^+$-SMA$^+$ cells).

The core of the infarct was generally less colonized by BMPCs, but hypoxia alone cannot explain this pattern of BMPC recruitment. In vivo monitoring of oxygenation revealed that after the initial severe hypoxia following coronary ligation, pO_2 at the core of the infarct recovered within 3 to 5 days to levels comparable to those before coronary ligation, before the maximal BMPC mobilization, which was at peak at 1 week.[56] The absence of organized vascularization at the infarct core strongly suggested that this reoxygenation was not derived from the microcirculation. Instead, our results indicated that the recovery of myocardial oxygen levels was a result of the combined effects of marked wall thinning and decreased oxygen consumption in the infarct and possibly from facilitated oxygen diffusion mediated by percolating extravascular erythrocytes.

We previously described extravascular percolation of erythrocytes in tissues as an effect of monocyte/macrophage proteolytic activity and penetration of the extracellular matrix, leaving behind "tunnels."[19] We speculate that in the biomechanically active heart muscle these "cracks" in the tissue may expand and accommodate increasingly more blood, as actually shown here histologically as blood pools. The presence of extravascular erythrocytes in compact and extended structures, sometimes crossing the myocardial wall from the ventricular cavity to the epicardium, was also described by others in mice with ventricular rupture (called "channels"[37] and found to be instrumental for this process[59]).

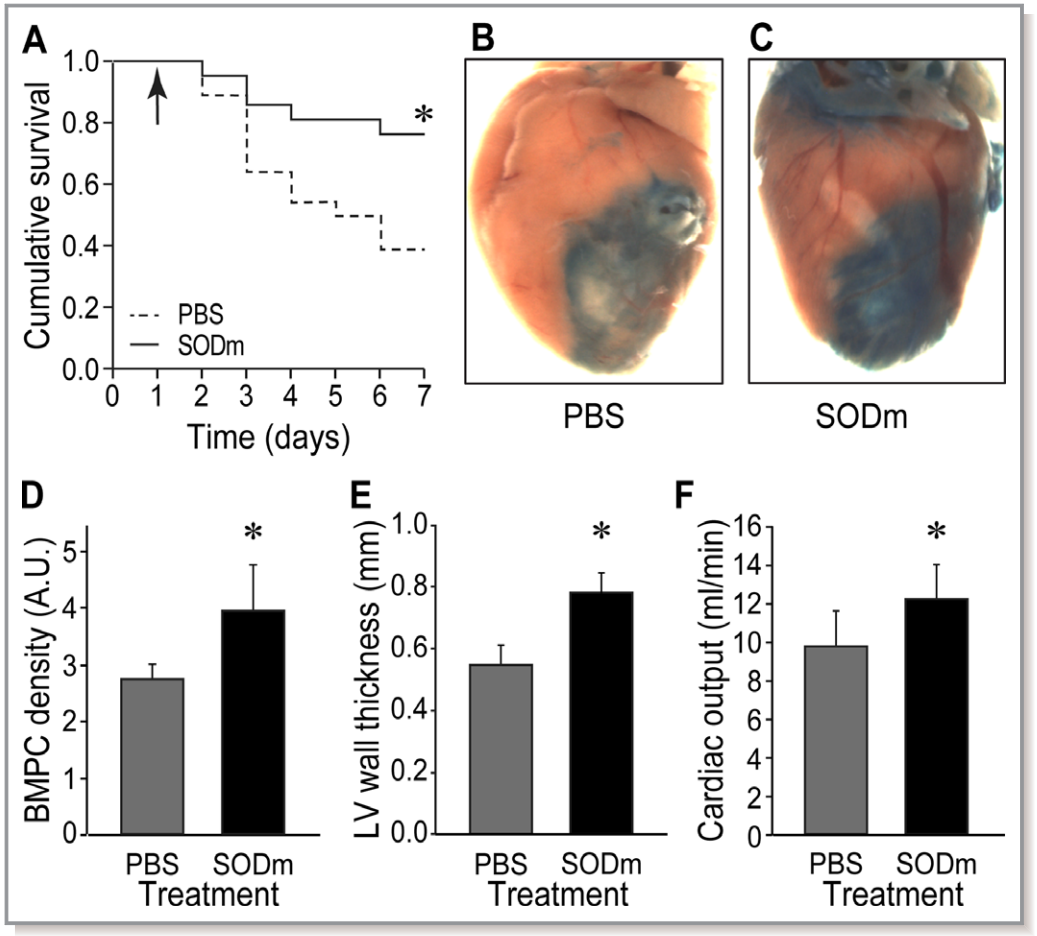

Figure 8. Cardiac structural and functional effects of in vivo antioxidant treatment (A). Kaplan–Meyer analysis of mice survival after coronary ligation. Solid line, mice treated with SODm (n=21); dashed line, controls (n=20); **P*=0.02 by log-rank statistical analysis (arrow, starting of treatment). B and C, Representative images of LacZ stained hearts from mice with bone marrow transplantation 7 days after coronary ligation to reveal areas of recruited BMPCs. B, Control heart. C, Heart of a mouse treated with SODm for 6 days after coronary occlusion; note the increased intensity of blue staining, indicative of increased BMPC recruitment in the infarct area (blue staining in the atrial region in this case is derived from the attached thymus). D, Semiquantitative image analysis of BMPC-derived β-galactosidase product on the surface of hearts in the control and SODm-treated mice (arbitrary units of blue color intensity). E, Minimum left ventricular wall thickness in control MI and SODm-treated MI mice 7 days after MI, as measured from gated cardiac MRI during diastole. F, Cardiac output in surviving mice that received SODm compared with those injected with vehicle-only (PBS), measured by gated cardiac MRI. D through F, Values are mean±SD (n=6 hearts per group); **P*<0.05. BMPC indicates bone marrow progenitor cell; LV, left ventricular; MI, myocardial infarction; MRI, magnetic resonance imaging.

A tunneling-based mechanism for translocation of resident progenitor cells themselves was proposed as well.[60]

Myocardial Reoxygenation Triggers ROS/RNS Formation

Thus, a key process in the passive reoxygenation of mouse hearts after permanent coronary ligation is wall thinning and concurrent mechanical failure leading to local microhemorrhages with erythrocyte percolation and, in a sizable proportion of mice, to ventricular rupture and death. One week after infarction the "ring" of BMPC engraftment was compactly distributed on the margin of the infarcted zone, whereas pools of erythrocytes were often noted in the central area. This segregation argues for different modes of tissue penetration of these blood-borne cells. Between 24 and 72 hours after coronary ligation, reoxygenation of the previously severely hypoxic infarct core occurred. Recovered oxygen delivery by both passive and perhaps facilitated diffusion from percolated red cells, along with likely decreased tissue oxygen consumption, could explain the higher oxygen levels observed. This late phase of postinfarction reoxygenation could support the enhanced ROS/RNS formation that occurs resulting in BMPC apoptosis, most marked at the infarct core. Although some controversy remains,[61] BMPCs and circulating stem/progenitor cells in particular have been found to be sensitive to overproduction of ROS.[62] In addition, endothelial progenitor cells are a site of peroxynitrite formation[48] with subsequent

reduction in survival.[63] Based on studies with inhibitors, this process of enhanced ROS/RNS formation was shown to be largely derived from iNOS and NADPH oxidase. Accordingly, in this study inhibition of iNOS and of NADPH oxidase markedly decreased measured ROS formation in the infarct core and border zone.

Antioxidant Treatment Enhances BMPC Engraftment, Cardiac Function, and Survival

We also found that antioxidant administration of an SOD mimetic in a window of opportunity starting 1 day after infarction (to avoid interference with natural recruitment of acute inflammatory cells) leads to substantial improvement of animal survival. At the macroscopic level, magnetic resonance imaging data showed that this was a result of decreased wall thinning with resulting biomechanical stabilization, reducing the incidence of rupture. At the microscopic level, increased engraftment and survival of BMPCs were coincident with decreased intramural hemorrhages and ventricular rupture, which in turn limited the increase in end-systolic and diastolic volumes of infarcted mouse hearts and increased their ejection fraction.[64] This is in accordance with prior reports on the beneficial effects of inhibition of ROS generation either in cardiomyocytes in situ[65] or in progenitor cells prior to use for cell therapy.[9]

The general protective role against ROS/RNS cytotoxicity of superoxide dismutase enzymes and mimetics, which also play a critical role in inhibiting oxidative inactivation of nitric oxide, thereby preventing peroxynitrite formation, is well documented.[66] The current report is the first to demonstrate the beneficial effects of pharmacological inhibition of superoxide formation in enhancing BMPC engraftment, myocardial resilience, and animal survival post-MI. With our observations that myocardial reoxygenation occurs post-MI, leading to stimulation of ROS/RNS generation from iNOS and NADPH oxidase, the protective effects of an SOD mimetic would be expected. These findings are consistent with our current data and those of others[47] demonstrating NT formation in engrafting cells and its association with their observed nuclear disintegration and apoptosis. Thus, SODm treatment dismutates superoxide, preventing peroxynitrite formation and secondary BMPC injury and death.

Limitations and Perspectives

Among the limitations of our study is that it was confined to the first week after permanent coronary ligation (7 days being both the peak of BMPC mobilization within the infarcted mouse heart[56] and of cardiac gp91^{phox} expression[47]). The true identity of the involved BMPCs, beyond their expression of LacZ or CD34, remains to be explored in more detail, as well as the contribution of inflammatory cells (including the role of the ROS they produce) to muscle microruptures and erythrocyte percolation. Another area of future in vitro and in vivo studies is the specific impact of SODm on BMPC functions in the context of their contribution to postinfarction events in the heart.

Conclusions

We observed that recruitment and survival of BMPCs in the infarct and border zone following MI are controlled by ROS/RNS that reduce the survival of BMPC in the process of engraftment. As depicted in Figure 9, the formation of these cytotoxic ROS/RNS is triggered by a reoxygenation that occurs from wall thinning, muscle microruptures, and extravascular erythrocytes that percolate through the myocardial wall. In the presence of these restored oxygen levels, the enzymes NOS2 (iNOS) and NADPH oxidase lead to the formation of cytotoxic levels of ROS/RNS. Pharmacological

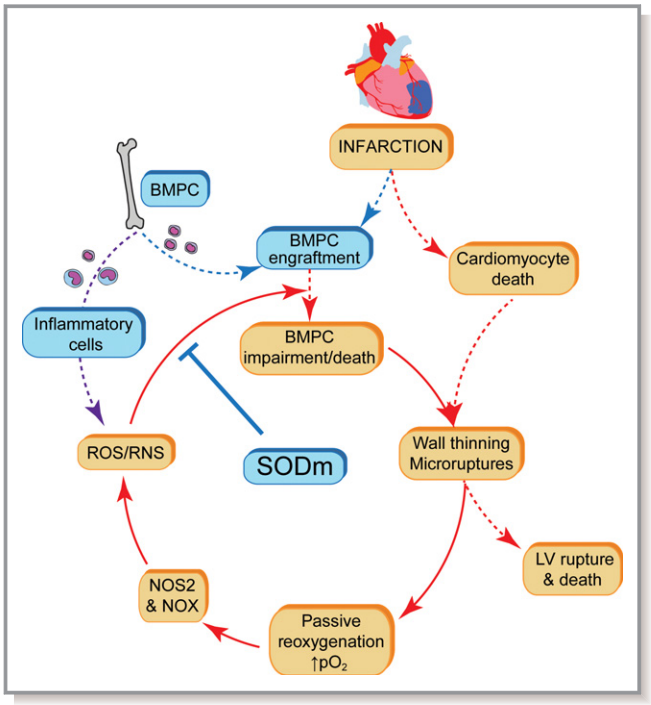

Figure 9. Mechanistic summary. Postinfarction recruitment and survival of BMPCs are limited by toxic ROS/RNS generated from reoxygenation due to wall thinning and muscle microruptures. Antioxidant treatment blocks ROS/RNS formation and preserves BMPC viability, allowing their protective functions (paracrine and/or fusion with cardiomyocytes or their differentiation into collagen-secreting myofibroblasts and other myocardial cells). These changes contribute to increased wall thickness and animal survival. Colors: red/orange, pathological processes; blue, reparative interventions. BMPC indicates bone marrow progenitor cell; LV, left ventricular; ROS/RNS, reactive oxygen/nitrogen species.

treatment with a SOD mimetic blocks ROS/RNS formation, in turn preventing BMPC death. We suggest that this intervention, by preserving BMPC viability, may allow their paracrine contribution to improved survival of cardiomyocytes, as well as their possible differentiation into collagen-secreting myofibroblasts or other myocardial cells. The favorable BMPC survival, engraftment, and differentiation may thus contribute to the noted increase in contractile function and wall thickness, with prevention of ventricular rupture, ultimately leading to increased survival.

Acknowledgments

The authors thank G. Marcucci for assistance with bone marrow transplantation, H. Talukder for assistance with animal experiments, and G. He for the initial oximetry measurements. Fluorescence imaging was done using the OSU Campus Microscopy and Imaging Facility.

Sources of Funding

This study was supported by American Heart Association Grant-In-Aid, HL65983 and HL96524 (to Dr Moldovan) and HL63744, HL65608, HL38324 and EB016096 (to Dr Zweier).

Disclosures

None.

References

1. Smith RR, Barile L, Messina E, Marban E. Stem cells in the heart: what's the buzz all about?—Part 1: preclinical considerations. *Heart Rhythm*. 2008;5:749–757.
2. Anversa P, Kajstura J, Rota M, Leri A. Regenerating new heart with stem cells. *J Clin Invest*. 2013;123:62–70.
3. Orlic D, Kajstura J, Chimenti S, Limana F, Jakoniuk I, Quaini F, Nadal-Ginard B, Bodine DM, Leri A, Anversa P. Mobilized bone marrow cells repair the infarcted heart, improving function and survival. *Proc Natl Acad Sci USA*. 2001;98:10344–10349.
4. Orlic D, Kajstura J, Chimenti S, Jakoniuk I, Anderson SM, Li B, Pickel J, McKay R, Nadal-Ginard B, Bodine DM, Leri A, Anversa P. Bone marrow cells regenerate infarcted myocardium. *Nature*. 2001;410:701–705.
5. Kawada H, Fujita J, Kinjo K, Matsuzaki Y, Tsuma M, Miyatake H, Muguruma Y, Tsuboi K, Itabashi Y, Ikeda Y, Ogawa S, Okano H, Hotta T, Ando K, Fukuda K. Nonhematopoietic mesenchymal stem cells can be mobilized and differentiate into cardiomyocytes after myocardial infarction. *Blood*. 2004;104:3581–3587.
6. Jackson KA, Majka SM, Wang H, Pocius J, Hartley CJ, Majesky MW, Entman ML, Michael LH, Hirschi KK, Goodell MA. Regeneration of ischemic cardiac muscle and vascular endothelium by adult stem cells. *J Clin Invest*. 2001;107:1395–1402.
7. Sam J, Angoulvant D, Fazel S, Weisel RD, Li RK. Heart cell implantation after myocardial infarction. *Coron Artery Dis*. 2005;16:85–91.
8. Cencioni C, Capogrossi MC, Napolitano M. The SDF-1/CXCR4 axis in stem cell preconditioning. *Cardiovasc Res*. 2012;94:400–407.
9. Pendergrass KD, Boopathy AV, Seshadri G, Maiellaro-Rafferty K, Che PL, Brown ME, Davis ME. Acute preconditioning of cardiac progenitor cells with hydrogen peroxide enhances angiogenic pathways following ischemia-reperfusion injury. *Stem Cells Dev*. 2013;22:2414–2424.
10. Ayach BB, Yoshimitsu M, Dawood F, Sun M, Arab S, Chen M, Higuchi K, Siatskas C, Lee P, Lim H, Zhang J, Cukerman E, Stanford WL, Medin JA, Liu PP. Stem cell factor receptor induces progenitor and natural killer cell-mediated cardiac survival and repair after myocardial infarction. *Proc Natl Acad Sci USA*. 2006;103:2304–2309.
11. Yang WJ, Li SH, Weisel RD, Liu SM, Li RK. Cell fusion contributes to the rescue of apoptotic cardiomyocytes by bone marrow cells. *J Cell Mol Med*. 2012;16:3085–3095.
12. Kishore R, Verma SK, Mackie AR, Vaughan EE, Abramova TV, Aiko I, Krishnamurthy P. Bone marrow progenitor cell therapy-mediated paracrine regulation of cardiac miRNA-155 modulates fibrotic response in diabetic hearts. *PLoS One*. 2013;8:e60161.
13. Prockop DJ. Mitochondria to the rescue. *Nat Med*. 2012;18:653–654.
14. Haudek SB, Xia Y, Huebener P, Lee JM, Carlson S, Crawford JR, Pilling D, Gomer RH, Trial J, Frangogiannis NG, Entman ML. Bone marrow-derived fibroblast precursors mediate ischemic cardiomyopathy in mice. *Proc Natl Acad Sci USA*. 2006;103:18284–18289.
15. van Amerongen MJ, Bou-Gharios G, Popa E, Van Ark J, Petersen AH, van Dam GM, van Luyn MJ, Harmsen MC. Bone marrow-derived myofibroblasts contribute functionally to scar formation after myocardial infarction. *J Pathol*. 2008;214:377–386.
16. van den Borne SW, Diez J, Blankesteijn WM, Verjans J, Hofstra L, Narula J. Myocardial remodeling after infarction: the role of myofibroblasts. *Nat Rev Cardiol*. 2010;7:30–37.
17. Hammerman H, Kloner RA, Hale S, Schoen FJ, Braunwald E. Dose-dependent effects of short-term methylprednisolone on myocardial infarct extent, scar formation, and ventricular function. *Circulation*. 1983;68:446–452.
18. Anzai A, Anzai T, Nagai S, Maekawa Y, Naito K, Kaneko H, Sugano Y, Takahashi T, Abe H, Mochizuki S, Sano M, Yoshikawa T, Okada Y, Koyasu S, Ogawa S, Fukuda K. Regulatory role of dendritic cells in postinfarction healing and left ventricular remodeling. *Circulation*. 2012;125:1234–1245.
19. Anghelina M, Krishnan P, Moldovan L, Moldovan NI. Monocytes/macrophages cooperate with progenitor cells during neovascularization and tissue repair: conversion of cell columns into fibrovascular bundles. *Am J Pathol*. 2006;168:529–541.
20. Ma Y, Halade GV, Lindsey ML. Extracellular matrix and fibroblast communication following myocardial infarction. *J Cardiovasc Transl Res*. 2012;5:848–857.
21. Rota M, Kajstura J, Hosoda T, Bearzi C, Vitale S, Esposito G, Iaffaldano G, Padin-Iruegas ME, Gonzalez A, Rizzi R, Small N, Muraski J, Alvarez R, Chen X, Urbanek K, Bolli R, Houser SR, Leri A, Sussman MA, Anversa P. Bone marrow cells adopt the cardiomyogenic fate in vivo. *Proc Natl Acad Sci USA*. 2007;104:17783–17788.
22. Rajasingh J, Thangavel J, Siddiqui MR, Gomes I, Gao XP, Kishore R, Malik AB. Improvement of cardiac function in mouse myocardial infarction after transplantation of epigenetically-modified bone marrow progenitor cells. *PLoS One*. 2011;6:e22550.
23. Khan M, Kutala VK, Wisel S, Chacko SM, Kuppusamy ML, Kwiatkowski P, Kuppusamy P. Measurement of oxygenation at the site of stem cell therapy in a murine model of myocardial infarction. *Adv Exp Med Biol*. 2008;614:45–52.
24. Obal D, Dai S, Keith R, Dimova N, Kingery J, Zheng YT, Zweier J, Velayutham M, Prabhu SD, Li Q, Conklin D, Yang D, Bhatnagar A, Bolli R, Rokosh G. Cardiomyocyte-restricted overexpression of extracellular superoxide dismutase increases nitric oxide bioavailability and reduces infarct size after ischemia/reperfusion. *Basic Res Cardiol*. 2012;107:305.
25. Ilangovan G, Li H, Zweier JL, Kuppusamy P. Electrochemical preparation and EPR studies of lithium phthalocyanine. 3. Measurements of oxygen concentration in tissues and biochemical reactions. *J Phys Chem B*. 2001;105:5323–5330.
26. Chacko SM, Khan M, Kuppusamy ML, Pandian RP, Varadharaj S, Selvendiran K, Bratasz A, Rivera BK, Kuppusamy P. Myocardial oxygenation and functional recovery in infarct rat hearts transplanted with mesenchymal stem cells. *Am J Physiol Heart Circ Physiol*. 2009;296:H1263–H1273.
27. Pandian RP, Parinandi NL, Ilangovan G, Zweier JL, Kuppusamy P. Novel particulate spin probe for targeted determination of oxygen in cells and tissues. *Free Radic Biol Med*. 2003;35:1138–1148.
28. Zhao X, He G, Chen YR, Pandian RP, Kuppusamy P, Zweier JL. Endothelium-derived nitric oxide regulates postischemic myocardial oxygenation and oxygen consumption by modulation of mitochondrial electron transport. *Circulation*. 2005;111:2966–2972.
29. Ismail JA, Poppa V, Kemper LE, Scatena M, Giachelli CM, Coffin JD, Murry CE. Immunohistologic labeling of murine endothelium. *Cardiovasc Pathol*. 2003;12:82–90.
30. Laurindo FR, Fernandes DC, Santos CX. Assessment of superoxide production and NADPH oxidase activity by HPLC analysis of dihydroethidium oxidation products. *Methods Enzymol*. 2008;441:237–260.

31. Chen CA, Wang TY, Varadharaj S, Reyes LA, Hemann C, Talukder MA, Chen YR, Druhan LJ, Zweier JL. S-glutathionylation uncouples eNOS and regulates its cellular and vascular function. *Nature*. 2010;468:1115–1118.
32. Duilio C, Ambrosio G, Kuppusamy P, DiPaula A, Becker LC, Zweier JL. Neutrophils are primary source of O_2 radicals during reperfusion after prolonged myocardial ischemia. *Am J Physiol Heart Circ Physiol*. 2001;280: H2649–H2657.
33. Ojha N, Roy S, Radtke J, Simonetti O, Gnyawali S, Zweier JL, Kuppusamy P, Sen CK. Characterization of the structural and functional changes in the myocardium following focal ischemia-reperfusion injury. *Am J Physiol Heart Circ Physiol*. 2008;294:H2435–H2443.
34. Aisagbonhi O, Rai M, Ryzhov S, Atria N, Feoktistov I, Hatzopoulos AK. Experimental myocardial infarction triggers canonical Wnt signaling and endothelial-to-mesenchymal transition. *Dis Model Mech*. 2011;4:469–483.
35. Fazel S, Cimini M, Chen L, Li S, Angoulvant D, Fedak P, Verma S, Weisel RD, Keating A, Li RK. Cardioprotective c-kit+ cells are from the bone marrow and regulate the myocardial balance of angiogenic cytokines. *J Clin Invest*. 2006;116:1865–1877.
36. Marban E. Big cells, little cells, stem cells: agents of cardiac plasticity. *Circ Res*. 2007;100:445–446.
37. Gao XM, Xu Q, Kiriazis H, Dart AM, Du XJ. Mouse model of post-infarct ventricular rupture: time course, strain- and gender-dependency, tensile strength, and histopathology. *Cardiovasc Res*. 2005;65:469–477.
38. Zweier JL, Flaherty JT, Weisfeldt ML. Direct measurement of free radical generation following reperfusion of ischemic myocardium. *Proc Natl Acad Sci USA*. 1987;84:1404–1407.
39. Garbett NC, Hammond NB, Graves DE. Influence of the amino substituents in the interaction of ethidium bromide with DNA. *Biophys J*. 2004;87:3974–3981.
40. Palomero J, Pye D, Kabayo T, Spiller DG, Jackson MJ. In situ detection and measurement of intracellular reactive oxygen species in single isolated mature skeletal muscle fibers by real time fluorescence microscopy. *Antioxid Redox Signal*. 2008;10:1463–1474.
41. Hansel TT, Kharitonov SA, Donnelly LE, Erin EM, Currie MG, Moore WM, Manning PT, Recker DP, Barnes PJ. A selective inhibitor of inducible nitric oxide synthase inhibits exhaled breath nitric oxide in healthy volunteers and asthmatics. *FASEB J*. 2003;17:1298–1300.
42. Dumitrescu C, Biondi R, Xia Y, Cardounel AJ, Druhan LJ, Ambrosio G, Zweier JL. Myocardial ischemia results in tetrahydrobiopterin (BH4) oxidation with impaired endothelial function ameliorated by BH4. *Proc Natl Acad Sci USA*. 2007;104:15081–15086.
43. Shimazu T, Otani H, Yoshioka K, Fujita M, Okazaki T, Iwasaka T. Sepiapterin enhances angiogenesis and functional recovery in mice after myocardial infarction. *Am J Physiol Heart Circ Physiol*. 2011;301:H2061–H2072.
44. Zweier JL, Talukder MA. The role of oxidants and free radicals in reperfusion injury. *Cardiovasc Res*. 2006;70:181–190.
45. Walter DH, Rittig K, Bahlmann FH, Kirchmair R, Silver M, Murayama T, Nishimura H, Losordo DW, Asahara T, Isner JM. Statin therapy accelerates reendothelialization: a novel effect involving mobilization and incorporation of bone marrow-derived endothelial progenitor cells. *Circulation*. 2002;105: 3017–3024.
46. Dewald O, Frangogiannis NG, Zoerlein M, Duerr GD, Klemm C, Knuefermann P, Taffet G, Michael LH, Crapo JD, Welz A, Entman ML. Development of murine ischemic cardiomyopathy is associated with a transient inflammatory reaction and depends on reactive oxygen species. *Proc Natl Acad Sci USA*. 2003;100: 2700–2705.
47. Zhao W, Zhao D, Yan R, Sun Y. Cardiac oxidative stress and remodeling following infarction: role of NADPH oxidase. *Cardiovasc Pathol*. 2009;18:156–166.
48. Ellis EA, Sengupta N, Caballero S, Guthrie SM, Mames RN, Grant MB. Nitric oxide synthases modulate progenitor and resident endothelial cell behavior in galactosemia. *Antioxid Redox Signal*. 2005;7:1413–1422.
49. Yang J, Ii M, Kamei N, Alev C, Kwon SM, Kawamoto A, Akimaru H, Masuda H, Sawa Y, Asahara T. CD34+ cells represent highly functional endothelial progenitor cells in murine bone marrow. *PLoS One*. 2011;6:e20219.
50. Carlson S, Trial J, Soeller C, Entman ML. Cardiac mesenchymal stem cells contribute to scar formation after myocardial infarction. *Cardiovasc Res*. 2011;91:99–107.
51. Kajstura J, Urbanek K, Rota M, Bearzi C, Hosoda T, Bolli R, Anversa P, Leri A. Cardiac stem cells and myocardial disease. *J Mol Cell Cardiol*. 2008;45:505–513.
52. Loffredo FS, Steinhauser ML, Gannon J, Lee RT. Bone marrow-derived cell therapy stimulates endogenous cardiomyocyte progenitors and promotes cardiac repair. *Cell Stem Cell*. 2011;8:389–398.
53. Jesty SA, Steffey MA, Lee FK, Breitbach M, Hesse M, Reining S, Lee JC, Doran RM, Nikitin AY, Fleischmann BK, Kotlikoff MI. c-kit+ precursors support postinfarction myogenesis in the neonatal, but not adult, heart. *Proc Natl Acad Sci USA*. 2012;109:13380–13385.
54. Wojakowski W, Landmesser U, Bachowski R, Jadczyk T, Tendera M. Mobilization of stem and progenitor cells in cardiovascular diseases. *Leukemia*. 2012;26:23–33.
55. Blomer N, Pachel C, Hofmann U, Nordbeck P, Bauer W, Mathes D, Frey A, Bayer B, Vogel B, Ertl G, Bauersachs J, Frantz S. 5-Lipoxygenase facilitates healing after myocardial infarction. *Basic Res Cardiol*. 2013;108:367.
56. Mouquet F, Pfister O, Jain M, Oikonomopoulos A, Ngoy S, Summer R, Fine A, Liao R. Restoration of cardiac progenitor cells after myocardial infarction by self-proliferation and selective homing of bone marrow-derived stem cells. *Circ Res*. 2005;97:1090–1092.
57. Mollmann H, Nef HM, Voss S, Troidl C, Willmer M, Szardien S, Rolf A, Klement M, Voswinckel R, Kostin S, Ghofrani HA, Hamm CW, Elsasser A. Stem cell-mediated natural tissue engineering. *J Cell Mol Med*. 2011;15:52–62.
58. Mollmann H, Nef HM, Kostin S, von Kalle C, Pilz I, Weber M, Schaper J, Hamm CW, Elsasser A. Bone marrow-derived cells contribute to infarct remodelling. *Cardiovasc Res*. 2006;71:661–671.
59. Nahrendorf M, Hu K, Frantz S, Jaffer FA, Tung CH, Hiller KH, Voll S, Nordbeck P, Sosnovik D, Gattenlöhner S, Novikov M, Dickneite G, Reed GL, Jakob P, Rosenzweig A, Bauer WR, Weissleder R, Ertl G. Factor XIII deficiency causes cardiac rupture, impairs wound healing, and aggravates cardiac remodeling in mice with myocardial infarction. *Circulation*. 2006;113:1196–1202.
60. Rota M, Padin-Iruegas ME, Misao Y, De Angelis A, Maestroni S, Ferreira-Martins J, Fiumana E, Rastaldo R, Arcarese ML, Mitchell TS, Boni A, Bolli R, Urbanek K, Hosoda T, Anversa P, Leri A, Kajstura J. Local activation or implantation of cardiac progenitor cells rescues scarred infarcted myocardium improving cardiac function. *Circ Res*. 2008;103:107–116.
61. Dernbach E, Urbich C, Brandes RP, Hofmann WK, Zeiher AM, Dimmeler S. Antioxidative stress-associated genes in circulating progenitor cells: evidence for enhanced resistance against oxidative stress. *Blood*. 2004;104:3591–3597.
62. Ingram DA, Krier TR, Mead LE, McGuire C, Prater DN, Bhavsar J, Saadatzadeh MR, Bijangi-Vishehsaraei K, Li F, Yoder MC, Haneline LS. Clonogenic endothelial progenitor cells are sensitive to oxidative stress. *Stem Cells*. 2007; 25:297–304.
63. Imanishi T, Hano T, Nishio I. Angiotensin II accelerates endothelial progenitor cell senescence through induction of oxidative stress. *J Hypertens*. 2005; 23:97–104.
64. Naumova AV, Chacko VP, Ouwerkerk R, Stull L, Marban E, Weiss RG. Xanthine oxidase inhibitors improve energetics and function after infarction in failing mouse hearts. *Am J Physiol Heart Circ Physiol*. 2006;290:H837–H843.
65. van Empel VP, Bertrand AT, van Oort RJ, van der Nagel R, Engelen M, van Rijen HV, Doevendans PA, Crijns HJ, Ackerman SL, Sluiter W, De Windt LJ. EUK-8, a superoxide dismutase and catalase mimetic, reduces cardiac oxidative stress and ameliorates pressure overload-induced heart failure in the harlequin mouse mutant. *J Am Coll Cardiol*. 2006;48:824–832.
66. Fukai T, Ushio-Fukai M. Superoxide dismutases: role in redox signaling, vascular function and diseases. *Antioxid Redox Signal*. 2011;15:1583–1606.